

Atomic Clocks and Coherent Population Trapping: Experiments for Undergraduate Laboratories

Nathan Belcher,¹ Eugeny E. Mikhailov,¹ and Irina Novikova¹

¹*Department of Physics, College of William & Mary, Williamsburg, Virginia 23185, USA*

(Dated: March 6, 2019)

We demonstrate how to construct and operate a simple and affordable experimental apparatus, appropriate for an undergraduate setting, in order to produce and study coherent effects in atomic vapor and to investigate their applications for metrology. The apparatus consists of a vertical cavity surface emitting diode laser (VCSEL) directly current-modulated using a tunable microwave oscillator to produce multiple optical fields needed for the observation of the coherent population trapping (CPT). This effect allows very accurate measurement of the transition frequency between two ground state hyperfine sublevels (a “clock transition”), that can be used to construct a CPT-based atomic clock.

PACS numbers:

INTRODUCTION

Coherent interactions of electromagnetic fields with atoms and molecules are attracting growing attention, as they enable coherent control and manipulation of quantum properties of light and matter. In particular, simultaneous interaction of atoms with two or more light fields allows all-optical addressing of the microwave transition between long-lived spin states of alkali metals, such as Rb or Cs. If the frequency difference of the two fields matches exactly the splitting between two hyperfine sublevels of atomic ground state, the atoms are prepared in a non-interacting coherent superposition of the two states, known as a “dark state”. This effect is known as coherent population trapping (CPT) [2]. Since the dark state exists only for very narrow range of differential frequencies between the two optical fields, a narrow transmission peak is observed when the frequency of either optical field is scanned near the resonance, so this effect is also often called electromagnetically induced transparency (EIT) [3]. There are a number of exciting and important applications of these effects, such as atomic clocks [4, 5] and magnetometers [6, 7], slow and fast light [8], quantum memory for photons [1, 9], nonlinear optics at the single photon level [10], etc. In recent years, EIT and related effects have gone beyond atomic systems and have been adopted for a wide range of more complex systems such as molecules, impurities in solid state crystals, quantum dots, optical microresonators, and other photonic structures.

While the idea of coherent control and manipulation of atomic and light quantum properties is becoming increasingly important in many areas of physics, there are only a few publications aimed at introducing undergraduate physics students to the concepts [11]. The complexity and high cost of conventional EIT equipment are the main obstacles in making these experiments more accessible for students with little or no experience in optics. Here, we present an experimental arrangement suitable

for an undergraduate laboratory, which allows students to observe EIT and study its properties, as well as to build an atomic clock and/or magnetometer by locking a microwave oscillator on clock resonance in Rb atoms.

BRIEF SUMMARY OF RELEVANT THEORY

Complete analytical treatment of EIT, which includes spontaneous transitions between different atomic levels, requires the density matrix formalism—a concept not generally introduced to undergraduate students. However, the essence of the effect can be easily demonstrated using wave functions, which are commonly used in undergraduate quantum mechanics courses [13].

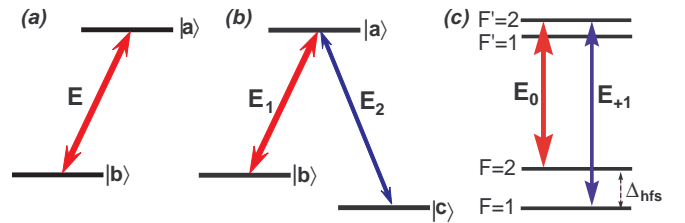


FIG. 1: Interaction of light with (a) two-level atom; (b) three-level atom in a Λ -configuration; and (c) realization of the Λ configuration for the D_1 line of ^{87}Rb . Here E_0 and E_{+1} are the carrier and the first high-frequency modulation sideband.

Let us first quickly review the important results regarding the interaction of a two-level atom with electromagnetic field, schematically shown in Fig. 1(a). In this case, an atom can be in any superposition of two atomic states ψ_a and ψ_b , which are eigenstates of unperturbed atomic Hamiltonian \hat{H}_0 , such that:

$$\hat{H}_0\psi_i = \hbar\omega_i\psi_i; \quad i = a, b. \quad (1)$$

Normally, all atoms are in their lower-energy (“ground”) state, but an oscillating electromagnetic field can vary

the populations by exciting atoms to the higher-energy (“excited”) state. Thus, we generally expect to find the system wave-function in the following form:

$$\Psi(t) = c_a(t)e^{-i\omega_a t}\psi_a + c_b(t)e^{-i\omega_b t}\psi_b, \quad (2)$$

where the coefficients $c_{a,b}(t)$ are functions of time, and the population of each atomic level (i.e., the probability to find an atom in this state) is determined by $|c_{a,b}(t)|^2$. To find these coefficients, we need to solve the time-dependent Schrödinger equation

$$i\hbar\frac{\partial\Psi(t)}{\partial t} = \hat{H}\Psi(t); \text{ where } \hat{H} = \hat{H}_0 + \hat{H}'. \quad (3)$$

The interaction part of the Hamiltonian \hat{H}' contains information about the interaction of atoms with the electromagnetic field $E(t) = \mathcal{E}\cos(\omega t)$. When the light is nearly resonant, i.e., its frequency ω is close to the frequency difference between two atomic states $\omega_{ab} = \omega_a - \omega_b$, it is convenient to use so-called *rotating wave approximation*. This approximation neglects the fast-oscillating part of the solution (proportional to $e^{\pm i(\omega + \omega_{ab})t}$), which averages out at the detection stage anyway, and keeps tracks of only measureable slow changes on the time scale proportional to $1/(\omega - \omega_{ab})$. In this case, the only two non-zero matrix elements of the interaction Hamiltonian are [13]:

$$\langle\psi_a|H'|\psi_b\rangle = H'_{ab} = \hbar\Omega e^{-i\omega t} \text{ and } H'_{ba} = \hbar\Omega e^{i\omega t}. \quad (4)$$

Here, Ω is proportional to the light field amplitude:

$$\Omega = \frac{\wp_{ab}\mathcal{E}}{2\hbar}, \quad (5)$$

and parameter $\wp_{ab} \equiv \langle\psi_a| -ez|\psi_b\rangle$ is the matrix element of the electron dipole moment; its value is determined by intrinsic properties of an atom and characterizes the strength of interaction with an external electromagnetic field.

To find the equations describing the time evolution of the state coefficients c_a and c_b , one needs to substitute the expression for the wavefunction (2) into the Schrödinger equation (3) and then use the orthogonality conditions for the wave-functions $\langle\psi_a|\psi_b\rangle = 0$, to find:

$$i\dot{c}_a = \Omega e^{i(\omega - \omega_{ab})t} c_b; \quad (6)$$

$$i\dot{c}_b = \Omega e^{-i(\omega - \omega_{ab})t} c_a. \quad (7)$$

The solution of these equations is well-known [13]: the atomic population cycles between the ground and excited states at the frequency $\sqrt{(\omega - \omega_{ab})^2 + \Omega^2}$. Such oscillations are called the Rabi flopping, and the parameter Ω usually called Rabi frequency.

So far we considered only *stimulated* transitions between two atomic states, when any jumps between two atomic states are caused solely by an electromagnetic

field. In this case, atoms repeatedly absorb and emit photons of the incident electromagnetic field, and no energy is lost in the process. It is important to emphasize that this picture is not completely accurate, since it does not take into account the finite lifetime of the excited state. When atoms are in the excited states, they can *spontaneously* decay into the ground state by emitting a photon in a random direction, so that the energy carried out by this photon is lost from the original light field. As a result, some fraction of resonant light is absorbed after the interaction with atoms.

Let us now return to the main topic of interest for our experiment: interaction of three-level atoms with two nearly-resonant laser fields, forming a Λ configuration shown in Fig. 1(b). In this case, the state of such an atomic system is generally given by a superposition of all three states:

$$\Psi(t) = c_a(t)e^{-i\omega_a t}\psi_a + c_b(t)e^{-i\omega_b t}\psi_b + c_c(t)e^{-i\omega_c t}\psi_c. \quad (8)$$

In all further discussion, we assume that the states $|\psi_b\rangle$ and $|\psi_c\rangle$ are metastable ground states (i.e., their lifetimes is considered very long), and the state $|\psi_a\rangle$ is the excited state, which decays to the ground states with the average lifetime $\tau_a = 1/\gamma_a$. We also assume that each of the electromagnetic fields interacts with only one atomic transition: the field $E_1(t) = \mathcal{E}_1\cos(\omega_1 t)$ couples the states $|\psi_a\rangle$ and $|\psi_b\rangle$, and the field $E_2(t) = \mathcal{E}_2\cos(\omega_2 t)$ couples the states $|\psi_a\rangle$ and $|\psi_c\rangle$. Mathematically, this means that the only non-zero matrix elements of the three-level system interaction Hamiltonian are $H'_{ab} = \hbar\Omega_1 e^{-\omega_1 t}$ and $H'_{ac} = \hbar\Omega_2 e^{-\omega_2 t}$ and their complex conjugates. Following the same steps as for a two-level system, we arrive to the following equations for the coefficients of the wavefunction (8):

$$i\dot{c}_a = \Omega_1 e^{i(\omega_1 - \omega_{ab})t} c_b + \Omega_2 e^{i(\omega_2 - \omega_{ac})t} c_c; \quad (9)$$

$$i\dot{c}_b = \Omega_1 e^{-i(\omega_1 - \omega_{ab})t} c_a; \quad (10)$$

$$i\dot{c}_c = \Omega_2 e^{-i(\omega_2 - \omega_{ac})t} c_a. \quad (11)$$

In these calculations, we have so far neglected the finite lifetime of the excited state $|\psi_a\rangle$. To properly account for it, one has to use more sophisticated density matrix formalism. However, it is intuitively clear that optical losses due to spontaneous emission should be proportional to the population of the excited state $|c_a|^2$. Thus, if somehow we can prevent atoms from getting excited, no energy will be dissipated, and the light field will propagate through atoms without any absorption. Let's examine Eq. 9 more closely and find the conditions at which $\dot{c}_a(t) = 0$ at all times. Physically, this corresponds to the situations when no atoms from either ground state are excited at any time, even in the presence of the light fields, and thus no light is absorbed. It is easy to see that this is possible only when:

$$\Omega_1 c_b = -\Omega_2 c_c e^{i[(\omega_2 - \omega_{ac}) - (\omega_1 - \omega_{ab})]t} \quad (12)$$

Since normally the phases of laser fields are constant, this equality requires that $(\omega_2 - \omega_{ac}) - (\omega_1 - \omega_{ab}) = 0$. This is can be rewritten as $\omega_2 - \omega_1 = \omega_{bc}$ and it is often called a *two-photon resonance*, since it specify *difference* in the frequencies of two light fields and the frequency splitting of two metastable states $\omega_{bc} = \omega_b - \omega_c$. At such a two-photon resonance, the atomic system can be prepared in the non-interacting quantum state that is completely decoupled from the excited state:

$$|D\rangle = \frac{\Omega_2 e^{-i\omega_b t} \psi_b - \Omega_1 e^{-i\omega_c t} \psi_c}{\sqrt{\Omega_1^2 + \Omega_2^2}} \quad (13)$$

Any atom in state $|D\rangle$ never gets excited to the level $|a\rangle$, and the atomic sample viewed from the side stays dark due to lack of the spontaneous emission. For that reason such a quantum state is often called a “dark state,” in which the atomic population is “trapped” in two lower states. Notice that the dark state is a *coherent* superposition of the two atomic states $|b\rangle$ and $|c\rangle$, sensitive to their relative phase. That exchange requires the two optical fields to maintain their relative phase at all times, in order for atoms to stay “invisible” to the light fields. That is why this effect is called *coherent* population trapping, to distinguish it from often non-coherent optical pumping.

Let’s now discuss what happens to light transmission if the frequency of one of the lasers is changing. Under the two-photon resonance conditions, the atomic medium is completely transparent. However, if the system is not exactly at the two-photon resonance and has a small two-photon detuning $\delta = \omega_2 - \omega_1 - \omega_{bc} \neq 0$, then the relative phase of the two states is slowly changing in time. If the two-photon detuning δ is small, we can still use the dark state formalism, except that such a “disturbed dark state”

$$|D\rangle = \frac{\Omega_2 e^{-i\omega_b t} \psi_b - e^{i\delta \cdot t} \Omega_1 e^{-i\omega_c t} \psi_c}{\sqrt{\Omega_1^2 + \Omega_2^2}} \quad (14)$$

stops being non-interacting after some time $\delta \cdot t \gtrsim 1$. After that, $\dot{c}_a > 0$, causing non-zero atomic population in the excited state, and thus increased absorption due to spontaneous emission.

In our analysis so far, we have allowed atoms to remain in the dark state infinitely long. In any real system, however, some decoherence mechanisms are always present to disturb a quantum state by randomizing its phase or even forcing atoms to jump between two random energy levels. Even under perfect two-photon resonance, atoms cannot be in the dark state longer than some characteristic dark state lifetime τ . Therefore, even for small non-zero two-photon detuning the transparency remains if the additional phase accumulated by the dark state during its “lifetime” is small $\delta \leq 1/\tau$. For larger two-photon detuning, the dark state no longer exists, and the amount of light absorption becomes large. So we can characterize

the width of the CPT resonance, i.e., the range of two-photon detunings where transmission is still high. The exact expression of the width can be found only using a more complete treatment:

$$\delta_{\text{CPT}} = \frac{1}{\tau} + \frac{|\Omega_1|^2 + |\Omega_2|^2}{\gamma_a}. \quad (15)$$

For stronger laser fields CPT resonance is broadened (“power broadened”), but the ultimate width is limited by the inverse lifetime of the dark state.

In the previous discussion, we talked about an idealized three-level atom, but no such atoms exist in nature. However, it is possible to realize a three-level Λ system very similar to one considered above in alkali metals. In these elements, two non-degenerate hyperfine states of the ground $nS_{1/2}$ level are used as states $|\psi_b\rangle$ and $|\psi_c\rangle$, and the electron state $nP_{1/2}$ or $nP_{3/2}$ becomes the excited state $|\psi_a\rangle$. Since spontaneous radiative decay between two hyperfine states of the same ground level is strictly forbidden, an atom can stay in either state until some interaction with its environment. Scientists now can preserve the quantum state of atoms for up to several seconds, but it require using cold atoms or exotic chemical coatings. In a regular vapor cell (i.e., a sealed glass cell filled with alkali metal vapor at about room temperature) the main limitation of the ground state lifetime is the motion of atoms: once an atom leaves the laser beam, it is likely to collide with the glass wall and thermalize (i.e., to lose any information about its previous quantum state and return to thermal equilibrium population distribution between two hyperfine states). For a 1 mm laser beam, the interaction time of an atom is limited by a few μs , which corresponds to a CPT linewidth of tens or even hundreds of kHz. Sometimes a buffer gas—usually a non-interacting inert gas—is added to the vapor cell together with alkali metal. In this case, alkali atoms diffuse through the laser beam rather than go ballistically, thus increasing the interaction time by a few orders of magnitude, and producing narrower CPT resonances.

EXPERIMENTAL SETUP

Diode lasers are an ideal choice for working with alkali metals (K, Rb, Cs) [12] since they are affordable, reliable and easy to operate, and cover the right spectral range. The exact output frequency of a diode laser can be fine-tuned by changing the driving current and/or the temperature of the diode. In our experiments, we use a laser resonant with the D_1 line of ^{87}Rb (wavelength $\lambda = 795 \text{ nm}$). However, a different Rb isotope or any other alkali metal can be used to reproduce the experiments described below with an appropriate change in the operational parameters.

The level structure of ^{87}Rb D_1 line is shown in Fig. 1(c). Both the ground ($5S_{1/2}$) and the excited

($5P_{1/2}$) states are split due to the coupling of the electron angular momenta and the nuclear spin, and each state is labeled with the value of the total angular momentum F . The observation of CPT requires two laser fields to couple both ground states $F = 1$ and $F = 2$ with the same excited state ($F' = 2$ for our experiments). However, it is impossible to use two independent diode lasers due to their relatively large intrinsic frequency noise. On one hand, a dark state (14) exists only if the differential frequency of two laser fields matches the ground-states splitting with good precision (typically better than a few kHz). On the other hand, the electromagnetic field emitted by a laser is not truly monochromatic, but instead its frequency “jumps” around randomly in a certain range (called a laser linewidth). If two independent lasers were used, their two-photon detuning would fluctuate in the range determined by the laser linewidths: a typical free-running diode laser (10 – 100 MHz), or even a more sophisticated external-cavity diode laser (≈ 1 MHz), which is too large compared to the expected width of a CPT resonance.

To avoid this problem we derive several electromagnetic fields from a single laser by modulating its phase $\varphi(t) = \epsilon \sin(\omega_m t)$. This is equivalent to producing a frequency comb with the frequency separation between the “teeth” equal to the modulation frequency ω_m , and the amplitude of each component determined by the phase modulation amplitude ϵ [14]:

$$\begin{aligned} E(z, t) &= \frac{1}{2} \mathcal{E} e^{ikz - i\omega t + i\varphi(t)} + c.c. \\ &= \frac{1}{2} \mathcal{E} \sum_{n=0}^{\infty} J_n(\epsilon) e^{ikx - i(\omega - n\omega_m)t} + c.c., \end{aligned} \quad (16)$$

In our experiments, we use two of the resulting frequency comb components—usually the zeroth (at the carrier frequency ω) and one of the first (at frequency $\omega \pm \omega_m$) modulation sidebands—to form a Λ system. To achieve CPT, the modulation frequency must be close to the hyperfine splitting frequency $\omega_m \approx \Delta_{\text{hfs}} = 6.835$ GHz. A special type of diode lasers—a vertical-cavity surface-emitting laser (VCSEL) [15]—allows efficient phase modulation at such high microwave frequency by directly modulating its driving current. For this type of laser an active region (where the lasing occurs) is smaller than in conventional edge-emitting diode lasers, providing two main advantages: fast response (up to 10 GHz modulation was achieved for our sample), and very low power consumption. Both of these properties make a VCSEL the laser of choice for miniature atomic clock applications [4].

Below we give a detailed description of the experimental apparatus constructed in our laboratory.

Laser assembly Fig. 2 shows the homemade laser head assembly used in our experiment. A VCSEL laser (ULM795-01-TN-S46FOP from U-L-M Photonics) is placed inside a collimating tube (model LDM 3756

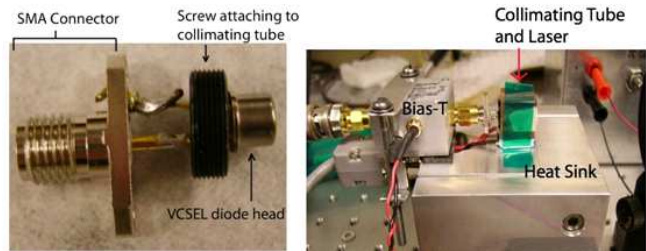


FIG. 2: (left) The VCSEL attached to an SMA connector. (right) The laser head assembly.

from Optima Precision) and a copper holder. The resulting assembly is attached to a thermoelectric cooler (TEC) connected to a temperature controller (model WTC3293-14001-A from Wavelength Electronics) to actively stabilize the diode temperature with precision better than 0.1°C . The sensitivity of the laser frequency to temperature (0.06 nm/ $^\circ\text{C}$ for our laser) introduces a means to tune the laser to the atomic resonance frequency, but also puts stringent requirements on the diode’s temperature stability. To prevent temperature fluctuations due to air currents, the laser mount is enclosed in a small aluminum box.

The laser diode pins are soldered to a standard SMA connector and plugged into a Bias-T (model ZFBT-6GW from Mini-Circuits), which combines a high-frequency modulation signal (see next section) and a constant current, required to drive the VCSEL. A typical driving current required to power VCSELs is very small (3 mA maximum allowed current in our sample). To extend the lifetime of the diode, we operated it at 1 – 1.5 mA, resulting in the output laser power of ≈ 0.5 mW, collimated to the 1 mm beam. Any variations in laser current also cause fluctuations in the output laser frequency (≈ 0.9 nm/mA); thus we have designed a simple, battery-operated, low-noise current supply optimized to drive a VCSEL (electric circuits are available in [16]). For the CPT and clock measurements, the output laser frequency is also actively locked to the atomic transition using a DAVLL technique [17, 18].

Microwave modulation In addition to a constant driving current, a high-frequency signal has to be mixed in to phase-modulate the output of the laser and produce the frequency comb given by Eq.(16). In our experiments, we tested a number of different microwave oscillators. For initial tests, we used a commercial frequency synthesizer (Agilent E8257D) available in our laboratory. However, for all later work, it was replaced with more economical options: a current-tunable crystal oscillator and an electronic phase-locked loop (PLL) with external 10 MHz reference.

The most affordable rf source was a Stellex Mini-YIG Oscillator purchased on eBay from a surplus electronic seller. This oscillator outputs 15 dBm of power at a fre-

frequency range between 5.95 GHz and 7.15 GHz. The output frequency of the oscillator can be tuned by changing the current flowing through two internal magnetic coils: a main coil, designed for coarse tuning of the oscillator frequency in a limited modulation bandwidth of about 10 kHz, and a fast tuning coil with the 400 kHz bandwidth. The tuning rates for the coils are 5 MHz/mA for the main coil and 150 kHz/mA for the fast tuning coil. As before, a current source used for tuning must have minimal internal noise (better than many commercial laser current drivers), since any modulation frequency fluctuations are immediately translated into fluctuations of the two-photon detuning. In our case, the tuning current required to reach the designed oscillator frequency (6.835 GHz) is relatively large > 100 mA. To simplify the construction of a tunable low-noise high-current source, we used a two-stage design: the oscillator frequency is coarsely set to the required value by manually adjusting a cw current source driving the main tuning coil to approximately 140 mA; an additional tunable low-current source plugged into the fast tuning coil is responsible for fine frequency adjustments in the narrow range of about 1 MHz around the set value. Electric circuits for the oscillator drivers are available in [16]. The described tuning source allows tuning the oscillator frequency to any particular microwave frequency or sweeping the modulation frequency to observe changes in optical transmission as a function of the two-photon detuning. While all the described experiments can be performed using the Stellex oscillator, it is sometimes not very convenient to use because of its large internal frequency jitter at the level of several tens of kilohertz. Also, without active frequency locking, its frequency drifts several hundreds kilohertz during an hour, probably because of its poor temperature stability.

The other microwave source we used requires more initial investments, but provides much greater precision and stability in the output frequency. It is based on the Linear PLL chip (LMX2487) evaluation board (LMX2487EVAL), which sets a user provided voltage controlled oscillator (VCO) at an arbitrary frequency near 6.835 GHz with sub-Hertz resolution (we used CRO6835Z). The output signal is phased-locked to a 10 MHz reference, and this feature can be used, for example, to lock the rf output to a stable frequency reference (such as a benchtop Rb frequency standard FS725 from SRS). Also, one can slightly vary the frequency of a voltage-controlled 10 MHz oscillator to achieve sweeping capability in the rf output frequency. We used a Streamline oscillator (501-04609A) with a voltage tuning response ± 5 Hz, corresponding to variation in the microwave frequency ± 3 kHz. This tuning is sufficient to lock the rf output to the CPT resonance and study its stability in an atomic clock arrangement.

The microwave output of either oscillator is connected to the laser through the bias-T, and the power of the os-

illator controls the strength of the modulation. Fig. 3(a) shows the modulation comb for two different values of rf power recorded by passing the laser output through a homemade Fabry-Perot cavity with 40 GHz free spectral range. Fig. 3(b) shows the ratio between the first and the zeroth (carrier) modulation sidebands grows proportionally to the microwave power sent to the VCSEL. Due to the high efficiency of the high-frequency current modulation, we were able to transfer a large fraction of optical power in the first modulation sideband, achieving the first sideband/carrier ratio > 1 for moderate modulation power ≥ 15 mW (12 dBm).

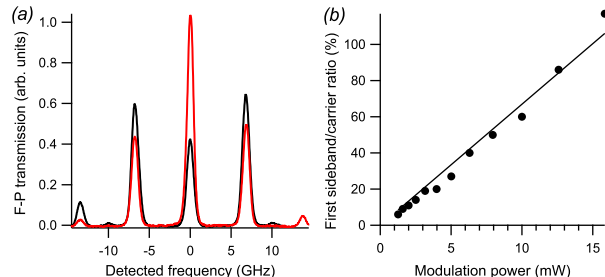


FIG. 3: (a) Frequency spectrum of the VCSEL modulated with 15 dBm and 10 dBm of rf power. (b) The dependence of the first sideband/carrier intensity ratio as a function of the rf power.

Rubidium cell enclosure The last remaining important component of the experimental setup is a Rubidium cell. In our experiment, we used a standard cylindrical glass cell (25 mm diameter, 75 mm length) containing isotopically pure ^{87}Rb . It is easy to estimate that at room temperature, Rb atoms inside the cell move with average speed of 400 m/s, spending in average only $2.5 \mu\text{s}$ inside the 1-mm laser beam. After that time, an atom most likely collides with the cell wall, and its quantum state created during the interaction with the laser fields is destroyed. To amend the situation, our cell also contains 5 Torr of Ne buffer gas (1 Torr \equiv 1 mmHg). Collisions with buffer gas atoms have a very weak effect on the atomic quantum state, but rapidly change the velocity of Rb atoms, restricting their motion to slow diffusion. As a result, Rb atoms spend much a longer time inside the interaction region, effectively increasing their dark state lifetime. For example, for Rb atoms in Ne buffer gas, the diffusion time of an atom through the laser beam diameter a can be approximated by the following expression:

$$\tau_{\text{diff}} = \frac{a^2}{1.15[\text{cm}^2/\text{s}] \frac{P_{\text{Ne}}}{P_{\text{atm}}}}, \quad (17)$$

where P_{Ne} is the pressure of Ne buffer gas inside the cell, and P_{atm} is the atmospheric pressure. For example, for the 1 mm beam used in the experiment, 5 Torr of Ne buffer gas extends interaction time from $2.5 \mu\text{s}$ to $60 \mu\text{s}$.

The exact total amount and composition of a buffer gas is not critical: any cell with 5 – 50 Torr of any inert gas (Ne, He, Ar, Xe) or some simple diatomic molecules (N_2 , CH_4) is suitable for the experiments described in the next sections.

Any longitudinal magnetic field splits the magnetic sublevels of all hyperfine states due to the Zeeman effect, and thereby changes their two-photon resonance frequencies. To avoid stray fields from the laboratory environment, the Rubidium cell is placed inside a set of three cylindrical magnetic shields to suppress any external magnetic field by a factor of $10^3 - 10^4$. However, much simpler single-layer shielding may be sufficient to observe CPT resonances of a few tens of kHz wide. It may also be useful to install a solenoid inside the shielding to controllably change the longitudinal magnetic field and study its effect on CPT.

The number of Rb atoms interacting with light (i.e. the Rb vapor density inside the cell) is determined by the saturated vapor pressure with the solid or liquid Rb metal droplet placed inside the cell, and can be controlled by changing the cell's temperature [12]. In our experiment, we control the temperature of the cell by passing constant electrical current through the resistive heater wrapped around the inner magnetic shield. To avoid any magnetic field due to the heater current, we used a bifilar chromium wire as a heating element; alternatively, any twisted loop of wire can be used, since the current will run in two opposite directions along each point of the wire. We found that the CPT resonances have the highest contrast at some optimal range of temperatures (35 – 50°C for our experiment): if the temperature is too low, almost all the light gets through regardless of CPT conditions, and if the temperature is too high almost it is hard to see CPT resonances due to strong absorption.

EXPERIMENT 1: OBSERVATION AND CHARACTERIZATION OF CPT RESONANCES

The described experimental apparatus enables a range of experiments that study coherent properties of atoms and their applications. The very first and basic one is the observation of CPT resonances by measuring the transmission of the laser light through the atomic cell while changing the laser modulation frequency scanned near two-photon resonance. The first step in this process is tuning the laser to the right optical frequency. Fig. 5 shows the transmission of the laser light when its frequency is swept across all four optical transitions of ^{87}Rb D_1 line [the transitions are shown in Fig. 1(c)]. The spectral width of each absorption lines is determined by the decoherence rate of the optical transitions of approx. 600 MHz FWHM (dominated by the Doppler broadening). As a result, the two transitions from the same ground state to each of the excited states are not

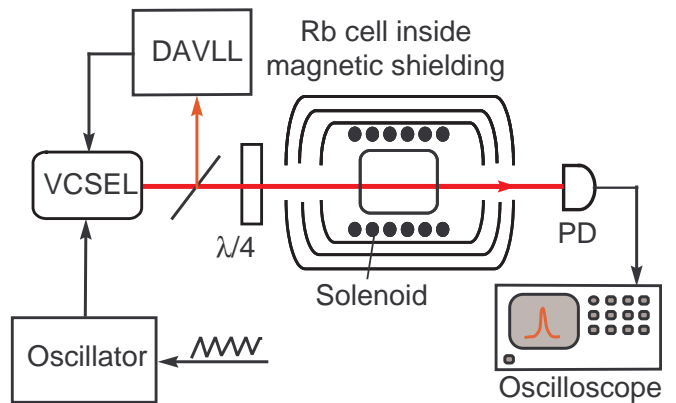


FIG. 4: Experimental setup for EIT observation. The radiation of a diode laser (VCSEL) passes through a quarter-wave plate ($\lambda/4$) and the shielded Rb cell, and any changes in its intensity are measured using a photodiode (PD) and a digital oscilloscope. The driving current of the laser is directly modulated using a tunable microwave oscillator. An additional laser lock (DAVLL) allows to maintain the laser frequency at the desired optical transition.

completely resolved, since their relatively small hyperfine splitting (≈ 800 MHz) is comparable to the width of each individual transition. The transitions from each of two ground states are clearly separated due to significantly larger ground-state hyperfine splitting ($\Delta_{\text{hfs}} = 6.835$ GHz).

The output optical frequency of the laser is sensitive to rf modulation power, and the precise tuning should be performed with modulation turned on. The tuning process is more convenient if the optical power in each of the first modulation sideband is $\approx 20 - 60$ % of the carrier field, so it is easy to distinguish the carrier and sideband absorption. Then the rf oscillator frequency should be appropriately tuned: first with the coarse tuning to the value of close to the hyperfine splitting, and then with fine adjustments such that a clear increase in light transmission is observed near Rb resonances, as illustrated by the difference in the solid lines in Fig. 5. To achieve the maximum contrast of CPT resonances with circularly polarized light, the carrier (i.e., the unperturbed laser frequency) should be tuned to the $F = 2 \rightarrow F' = 2$ transition; in this case, the high-frequency modulation sideband is resonant with the $F = 1 \rightarrow F' = 2$. This arrangement is indicated with an arrow in Fig. 5.

Once the laser optical frequency is parked at the right transition, one can directly observe a CPT resonance by slowly scanning the modulation frequency near the two-photon transition. Fig. 6 shows examples of narrow (a few kHz) peaks in the transmitted light power after the Rb cell when the CPT condition is fulfilled. Since all the laser light is detected, the CPT transmission peak is observed on top of an often large background. This background transmission consists of the off-resonant modula-

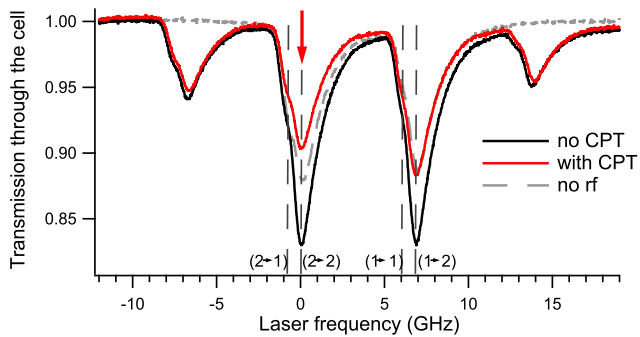


FIG. 5: Dependence of total laser transmission through the cell without rf modulation (dashed line) and with the rf modulation frequency tuned to the CPT resonance conditions (solid red line) and 2 MHz away from the CPT resonance (solid black line). The sideband/carrier ratio is 20%, and the laser power is $150 \mu\text{W}$. The positions of all four optical transitions for the carrier field are labeled and marked with vertical lines. Red arrow indicates the laser frequency used in all following measurements.

tion sidebands, which do not interact with atoms, as well as residual transmission of the resonant light fields, if the atomic density is not too high. It is also easy to see that even the maximum of the CPT resonance does not reach 100% transmission, since the lifetime of the dark state is finite, and there is always a fraction of atoms in the laser beam that is absorbing light. The exact position of the transmission maximum depends on many parameters, such as the power of the light (“light shift”), and the amount and the temperature of the buffer gas (“pressure shift”). For example, in the cell we used in the experiments (filled with 5 Torr of Ne) the position of the two-photon resonance at low light level was measured to be 6.83468512 GHz .

After initial detection of CPT resonances, it may be useful to systematically study the important properties, such as the effect of the laser power. For example, Eq. 15 predicts the broadening of CPT resonances at higher laser powers. It is easy to verify this experimentally by measuring the resonance width while reducing the light power interacting with atoms by placing (for example) a few neutral density filters in front of the cell. The example of the resonance narrowing is shown in Fig. 6. Note, however, that the resonance linewidth may not follow the Eq. 15 exactly, especially for moderate buffer gas pressure ($\leq 10 \text{ Torr}$), since the dynamics of atomic diffusion becomes important. In particular, if atoms are allowed to diffuse out of the laser beam and then return without losing their quantum state, the width of the CPT resonances may become much narrower than expected from the simple diffusion picture, provided by Eq. 17 [19].

One can also observe that the CPT resonance lineshape becomes asymmetric when the optical laser frequency is detuned from exact optical transition frequency [20].

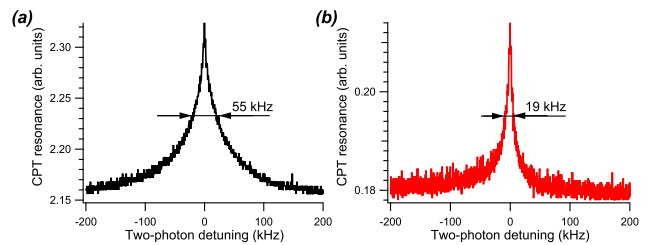


FIG. 6: CPT transmission resonances observed by sweeping the rf modulation frequency in a 400 kHz range around the 6.83468512 GHz for two values of the laser power: (a) $132 \mu\text{W}$ and (b) $32 \mu\text{W}$.

This effect can be used to fine-tune the laser frequency to the resonance position, which corresponds to the most symmetric CPT resonance. At the same time, students may find it interesting to observe this systematic lineshape change, accompanied by the reduction of the resonance amplitude and growth in background transmission as fewer and fewer atoms interact with the laser fields.

EXPERIMENT 2: EFFECT OF THE ZEEMAN STRUCTURE ON CPT RESONANCES; ATOMIC MAGNETOMETER

So far we have ignored the fact that each hyperfine sub-level F consists of $2F + 1$ magnetic (Zeeman) sublevels m_F . These sublevels are degenerate for zero magnetic field, but if a magnetic field is applied along the light propagation direction (for example, by running the current through the solenoid mounted inside the magnetic shielding), they shift by an amount proportional to the applied magnetic field B :

$$\delta_{m_F} = m_F g_F B, \quad (18)$$

where m_F is the magnetic quantum number for each sub-level, and g_F is the gyromagnetic ratio. For Rb levels the gyromagnetic ratios are quite small ($g_{F=1} = 0.7 \text{ MHz/G}$ and $g_{F=2} = -0.7 \text{ MHz/G}$), and rather high magnetic field is required to shift the levels far enough to resolve individual optical absorption resonances from different Zeeman sublevels. CPT resonances, on the other hand, are much more sensitive to level shifts.

Let’s look more carefully at what happens to a CPT resonance in the presence of magnetic field. Fig. 7(a) shows the relevant Rb energy levels taking into account their magnetic structure. In this case, we must consider not one, but three independent Λ systems formed by carrier and high-frequency sideband fields between three pairs of magnetic sublevels $m_f = 0, \pm 1$ in the ground states and magnetic sublevels $m_f = 0, 1$ and 2 (or $m_f = 0, -1$ and -2 depending on which circular polarization is used). When these levels are degenerate (no magnetic field) the dark state is formed at each pair of

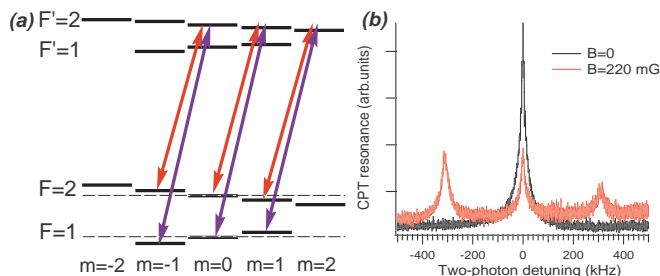


FIG. 7: (a) Level diagram for D₁ line of ^{87}Rb showing the Zeeman sublevels. (b) CPT resonance at zero magnetic field and for $B = 220$ mG.

ground state sublevels at the same rf frequency Δ_{hfs} . If the oscillator frequency is swept around this value, only one CPT peak is observed. However, in the presence of an applied magnetic field, the magnetic sublevels with different magnetic quantum numbers m_f shift by different amounts, as shown in Fig. 7(a). Now, the conditions for the two-photon resonance at Δ_{hfs} are obeyed only for non-shifted $m_F = 0$ pair, while for $m_F = \pm 1$ the resonance occurs now at $\Delta_{\text{hfs}} \pm 2g_F B$. As a result, the original single CPT peak splits into three peaks, as shown in Fig. 7(b). The frequency difference between the peaks is proportional to the applied magnetic field, and can be used as a sensitive magnetometer.

EXPERIMENT 3: CPT-BASED ATOMIC CLOCKS

Before discussing the application of CPT resonances for atomic clocks, it may be helpful to refresh the modern definition of the second: *The second is the duration of 9 192 631 770 periods of the radiation corresponding to the transition between the two hyperfine levels of the ground state of the Cesium-133 atom* [21]. This means that we have to accurately measure the frequency between two hyperfine states of Cs, and then count the given number of oscillations to determine the duration of one second. For clocks, it does not matter much if another alkali metal atom is used instead of Cs, since the hyperfine splitting of most of them is currently known with great precision. Thus, the principle of any atomic clock is simple: a frequency of some rf oscillator has to be locked to match the frequency difference between two hyperfine states of Cs or Rb (“clock transition”), and then the oscillation periods of this locked oscillator can be used as tick marks for measuring time. The international time standard at NIST—a Cs fountain clock—operates on this principle by directly probing the clock transition using microwave radiation. Of course, extreme care is taken in this case to avoid any systematic errors in frequency measurements to ensure current relative stability approaching 10^{-17} level.

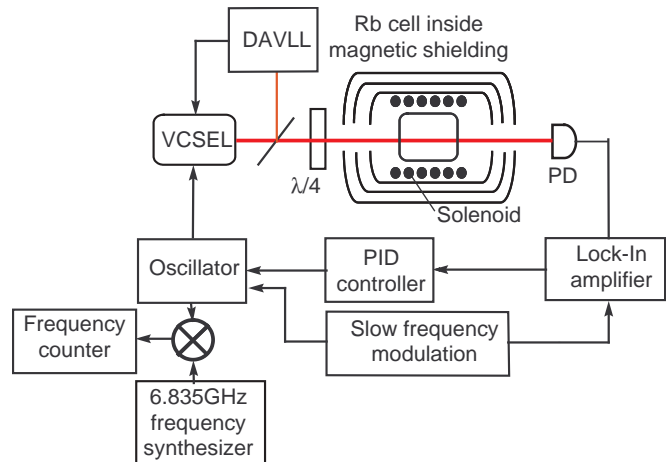


FIG. 8: Experimental setup for atomic clocks. Most elements are the same as for Fig. 4, except that now the output of the photodetector is used in the feedback loop to lock the microwave oscillator frequency at the peak of a CPT resonance. Small fraction of the oscillator output is then mixed with external reference oscillator to measure the stability of the resulting atomic clocks.

However, many practical applications could benefit from an atomic clock whose stability is only at the level of $10^{-12} - 10^{-13}$, so long as such a device is compact, robust, and power-efficient. In particular, CPT resonances are very attractive for the development of miniature atomic clocks, since all optical components can be miniaturized without loss in performance [7], and no bulky rf cavity is needed. Since the CPT resonance occurs exactly when the frequency difference between two optical fields matches the hyperfine splitting in Rb (the clock transition), a CPT-based atomic clock can be constructed by locking the rf oscillator, used to modulate the VCSEL, to the maximum transmission through the atomic cell.

To realize such feedback in our experiment, a few additional pieces of equipment have been added to the setup, as shown in Fig. 8. First, a slow dithering modulation (5 – 10 kHz) was superimposed on top of the oscillator rf frequency. When the oscillator frequency is within a CPT resonance, this modulation induces corresponding modulation in the output optical transmission. Phase-sensitive detection of this signal, using a lock-in amplifier, transforms a symmetric transmission peak to an anti-symmetric error signal, which is zero at precisely the maximum of the CPT resonance. This error signal is then fed back to the tuning current of the oscillator to correct its frequency and prevent it from drifting away from clock transition frequency.

To evaluate the performance of the constructed atomic clock we need to measure the frequency stability of the locked oscillator. Since microwave equipment able to directly measure 6.8 GHz frequency is generally very expensive, we) we split a few percent of the oscillator out-

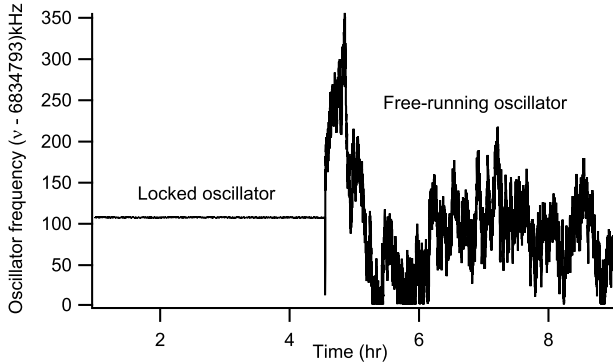


FIG. 9: The oscillator when optical and rf locked versus free-running.

put, mix it down to a few megahertz range by using a stable reference frequency source at the similar frequency. This signal can now be measured using a standard frequency counter. The difference in performance for the noisy Stellex oscillator when it free-running or when it is locked to the CPT resonances makes the advantage of a CPT-based atomic clock more striking, as illustrated in Fig. 9. It is easy to see a significant difference in oscillator stability: while the frequency of the free-running oscillator fluctuates by ± 175 kHz; the locked oscillator is stable within ± 2 Hz.

A common measure of an oscillator stability is the Allan variance [22]. To calculate the Allan variance one has to break up the whole set of frequency measurements into n sampling periods of the duration τ , and then to calculate the average frequency value ν_i for each i^{th} interval. Then the sum of squared differences between the two consecutive sampling periods $(\nu_{i+1} - \nu_i)^2$ is a good quantitative measure of the variation of the average frequency during the time τ . The precise mathematical expression for the Allan variance is the following:

$$\sigma^2(\tau) = \frac{1}{2(n-1)} \sum_{i=0}^{n-1} (\nu_{i+1} - \nu_i)^2. \quad (19)$$

The Allan variance depends on the averaging time τ , it is usually displayed as a graph. The lower the Allan variance, the better the stability of the oscillator. For a very stable but noisy oscillator the value of the Allan variance steadily improves with larger τ , since longer integration time reduces the effect of random noise. However, any long-term systematic drift causes the Allan variance to grow once the duration of the sampling period becomes comparable with the characteristic drift time. Typically, the minimum in the Allan variance plot indicates the optimal averaging time for the given experiment.

Fig. 10 shows the Allan variance calculated for the frequencies of the locked and the free-running oscillator. This plot clearly demonstrates close to four orders of magnitude improvement in the oscillator performance,

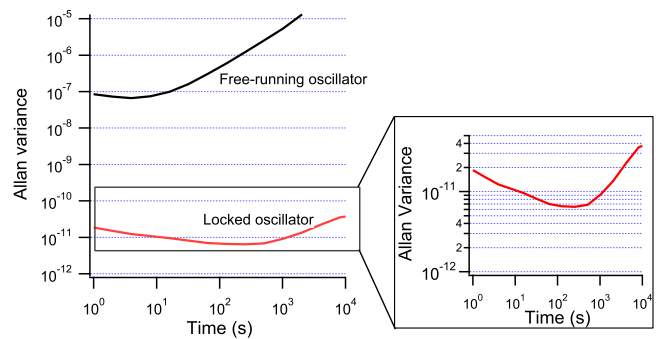


FIG. 10: Allan variance with the clock locked (red) and free-running (black).

from 9×10^{-8} over a time period of 10 seconds in the free-running regime, to 8×10^{-12} over 100 seconds in the regime of the CPT-based atomic clocks. To put this into perspective, if we could keep our clock that stable for a long enough time period, we would lose 1 second every 4000 years. We also measure how long our clock stays locked to microwave clock transition: our best attempt yielded a locking time of 41 hours with a 6 Hz drift, that was most likely limited by the quality of the DAVLL optical lock.

CONCLUSIONS

In this paper, we have presented details for the construction of an affordable and versatile experimental apparatus for observation coherent effects in an atomic vapor suitable for the undergraduate laboratory. In fact, assembly and debugging the apparatus is an appropriate task for a senior research project (the experimental apparatus described here was mainly designed and assembled by one of the co-authors (NB) during his senior year at the college of William & Mary). Work with this apparatus will allow students to learn the basics of diode lasers, rf equipment and atomic spectroscopy. We also described three possible experiments that can be realized using this apparatus. First, we described the procedure for observation of CPT transmission resonance due to manipulations of the coherent state of atoms. Then we take advantage of extreme sensitivity of the CPT resonance frequency to small shifts in the energy levels of atoms to measure small magnetic field. Finally, we lock the rf oscillator frequency to the CPT resonance using a feedback mechanism to create a prototype atomic clock. In addition, the same apparatus can be used for experiments devoted to slow and stored light experiment if the amplitude of the microwave radiation can be shaped into probe pulses.

It is important to note that all proposed activities are actively studied in research laboratories around the world, and they are discussed in reputable scientific jour-

nals. More generally, the ability to manipulate quantum states of an atom using light gave rise to several important applications, such as quantum memory and slow light, that are currently one of the most active and interdisciplinary areas of physics. Familiarity with the basics of these effects through the hand-on experience will be very beneficial for any undergraduate student.

ACKNOWLEDGEMENTS

The authors would like to thank Sergey Zibrov for advice on the experimental apparatus design, Chris Carlin for the help with laser lock construction, and Nate Phillips and Joe Goldfrank for useful feedback on this manuscript. This research was supported by Jeffress Research grant J-847, the National Science Foundation and the College of William & Mary.

-
- [1] M. D. Lukin, *Rev. Mod. Phys.* **75**, 457 (2003).
 [2] E. Arimondo, *Prog. Opt.* **35**, 257 (1996).
 [3] M. Fleischhauer, A. Imamoglu, and J. P. Marangos *Rev. Mod. Phys.* **77**, 633 (2005).
 [4] J. Vanier, *Appl. Phys. B* **81**, 421 (2005).
 [5] J. Comparo, *Phys. Today* **60**(11), 33 (2007).
 [6] M. Fleischhauer and M. O. Scully, *Phys. Rev. A* **49**, 1973 (1994).
 [7] P. D. D. Schwindt, S. Knappe, V. Shah, L. Hollberg, J. Kitching, L.-A. Liew, and J. Moreland, *Appl. Phys. Letts.*, **85**, 6409, (2004).
 [8] R. W. Boyd and D. J. Gauthier, in *Progress in Optics***43**, E. Wolf, Ed. (Elsevier, Amsterdam, 2002).
 [9] M. D. Eisaman, M. Fleischhauer, M. D. Lukin, and A. S. Zibrov, *Optics & Photonics News* **17**, 22 (2006).
 [10] M. D. Lukin and A. Imamoglu, *Phys. Rev. Lett.* **84**, 1419 (2000).
 [11] D. Budker, D. J. Orlando, and V. V. Yashchuk, *Am. J. Phys.* **67**, 584 (1999).
 [12] D. A. Steck. *Alkali D Line Data*, <http://steck.us/alkalidata/> (accessed September, 2008).
 [13] D. J. Griffiths, *Introduction to Quantum Mechanics* (Pearson Prentice Hall, Upper Saddle River, NJ, 2005), 2nd. ed.
 [14] G. B. Arfken and H. J. Weber, *Mathematical Methods for Physicists*, (Harcourt: San Diego, 2005), 6th ed.
 [15] C. Affolderbach, A. Nagel, S. Knappe, C. Jung, D. Wiedenmann, and R. Wynands, *Appl. Phys. B* **70**, 407 (2000).
 [16] N. Belcher, *Development of a Prototype Atomic Clock Based on Coherent Population Trapping*, B.S. Thesis, Department of Physics, The College of William & Mary (May, 2008); available at <http://ixnovi.people.wm.edu/publications/ClockDocs.html> (accessed September, 2008).
 [17] K. L. Corwin, Z.-T. Lu, C. F. Hand, R. J. Epstein, and C. E. Wieman, *Appl. Optics* **37**, 3295 (1998).
 [18] V.V. Yashchuk, D. Budker, and J. Davis, *Rev. Sci. Instr.* **71**, 341 (2000).
 [19] Y. Xiao, I. Novikova, D. F. Phillips, and R. L. Walsworth, *Phys. Rev. Lett.* **96**, 043601 (2006).
 [20] E. E. Mikhailov, I. Novikova, Y. V. Rostovtsev, and G.R. Welch, *Phys. Rev. A* **70**, 033806 (2004).
 [21] The official site of Bureau International des Poids et Mesures: http://www.bipm.org/en/si/base_units/ (accessed August, 2008).
 [22] D. W. Allan, *Allan Variance*, <http://www.allanstime.com/AllanVariance/> (accessed September, 2008).